Quasi-confocal fluorescence sectioning with dynamic speckle illumination

Cathie Ventalon and Jerome Mertz

Department of Biomedical Engineering, Boston University, 44 Cummington Street, Boston, Massachusetts, 02215

Received July 18, 2005; revised manuscript received September 5, 2005; accepted September 6, 2005

We present a simple modification to a conventional wide-field fluorescence microscope that provides depth discrimination in thick tissues. The technique consists of illuminating a sample with a sequence of independent speckle patterns and displaying the rms of the resultant sequence of fluorescence images. The advantage of speckle illumination is that it provides diffraction-limited illumination granularity that is highly contrasted even in scattering media. We demonstrate quasi-confocal imaging in a mouse olfactory bulb labeled with green fluorescent protein. © 2005 Optical Society of America

OCIS codes: 180.1790, 180.2520, 180.6900.

The main advantage of confocal fluorescence microscopy[1] over wide-field microscopy is that it provides optical sectioning, i.e., allows depth discrimination inside samples. Standard implementations of confocal microscopes require scanning of one or more illumination spots and are often technically elaborate. Nonscanning alternatives have been proposed.[2–4] In particular, structured light microscopy involves illuminating the sample with an incoherent structured light pattern (e.g., using a one-dimensional grid), and computing the image rms as the grid pattern is laterally displaced.[3,4] This effective technique confers the same sectioning property as a confocal microscope but is less adapted to thick tissue imaging as the pattern contrast is degraded by scattering. In this Letter we implement a similar technique where the incoherent grid pattern is replaced by a coherent speckle pattern. We demonstrate quasi-sectioning and argue that our technique is better adapted for thick tissue imaging because the speckle contrast, which arises from the summation of random optical phases, is maintained over a large depth of field even in scattering tissue.

The use of speckle illumination for optical sectioning has been suggested before. For example, nonfluorescence techniques have made use of the short axial correlation of speckle patterns to provide depth discrimination.[5,6] More recently, wide-field nonscanning fluorescence confocal microscopy has been demonstrated with a technique that requires an independent recording of the speckle illumination pattern inside the sample.[7,8] This method is technically challenging and cannot be used in scattering media. In this Letter we present a technique that is simple, robust, and applicable to imaging in thick tissue.

Our experimental setup consists of a standard wide-field microscope with an argon laser source ($\lambda = 488$ nm) delivering an average power of 3 mW into the sample (see Fig. 1). A diffuser plate in the laser beam path is imaged onto the back aperture of the objective and rotated with a stepper motor to produce dynamic speckle illumination (DSI). The images are recorded using a CCD camera (Retiga 2000R, Q-Imaging) chosen for its large well capacity. All our experiments were performed with an Olympus PLAN 60× water immersion objective of focal length $f = 3$ mm and numerical aperture NA = 0.9.

The inset in Fig. 1 illustrates the laser light inside the sample. The field of illumination, demarcated by the dotted curves, has a diameter $D \approx 300$ μm at the objective focal plane (dashed line). The small elongated ellipsoids depict the speckle pattern. The size of a speckle grain at an axial distance z from the focal plane is roughly $\lambda/\theta(z)$, where $\theta(z)$ is the angle subtended by all the rays incident on the grain (emanating from the diffuser plate). From simple geometric considerations (assuming $f \gg D$), the speckle size is found to be roughly constant over a depth of field $|z| \leqslant D/\mathrm{NA}$, corresponding to the region where $\theta(z)$ spans the full objective pupil.

The origin of sectioning can be understood from the inset in Fig. 1. The solid lines depict the detection point spread function ($\mathrm{PSF}_{\mathrm{det}}$) as seen by an arbitrary point at the CCD camera. Speckle illumination induces granular fluorescence that appears highly contrasted at the focal plane but blurred elsewhere. A random shift in the speckle pattern thus leads to a large variation in the in-focus light (depending on whether a speckle grain overlaps $\mathrm{PSF}_{\mathrm{det}}$) and a small variation in the out-of-focus blurred light. Consequently, a processing algorithm that extracts the variations in a sequence of images preferentially reveals signal arising from the focal plane and hence provides sectioning. In our case this algorithm is simply the rms of the image sequence.

A theoretical description of our technique is obtained by considering the fluorescence intensity incident on the detector plane, given by

$$I_d(\vec{\rho}_d) = \int\int \mathrm{PSF}_{\mathrm{det}}(\vec{\rho}_d - \vec{\rho}, -z) C(\vec{\rho}, z) I_s(\vec{\rho}, z) \mathrm{d}^2\vec{\rho}\,\mathrm{d}z, \tag{1}$$

where $I_s(\vec{\rho}, z)$ is the speckle intensity in the sample and $C(\vec{\rho}, z)$ is the fluorescent marker concentration (for simplicity we consider unit magnification). Detection and illumination PSFs (denoted $\mathrm{PSF}_{\mathrm{det}}$ and $\mathrm{PSF}_{\mathrm{ill}}$) are normalized such that $\mathrm{PSF}(0,0) = 1$ and $\int \mathrm{PSF}(\vec{\rho}, z) \mathrm{d}^2\vec{\rho} = A$.

To estimate the sectioning strength of our technique, we consider a thin uniformly fluorescent plane

0146-9592/05/243350-3/$15.00

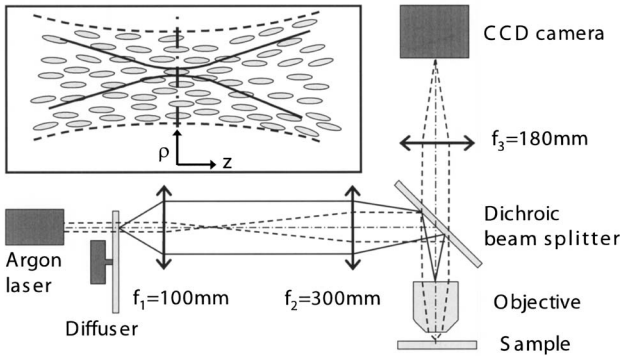

Fig. 1. Experimental setup. Laser light emanating from a rotating diffuser plate is imaged onto the back aperture of an objective and produces speckled illumination in the sample. The resultant fluorescence is imaged by a CCD camera. The inset depicts the laser light in the sample around the objective focal plane ($z=0$). Expansion lenses f_1 and f_2 are chosen such that the laser beam fills the objective back aperture.

$[C(\vec{\rho},z)=C\delta(z-z_c)]$ and calculate the expected intensity variance on each CCD pixel as a function of the axial position z_c of the fluorescent plane. The signal variance is defined by $V(\vec{\rho}_d)=\langle I_d(\vec{\rho}_d)^2\rangle-\langle I_d(\vec{\rho}_d)\rangle^2$, where the angular brackets denote averaging over independent speckle patterns. Since the setup exploits a wide-field Koehler illumination, the average speckle intensity is roughly constant over the field of illumination and throughout the large depth of field. That is, $\langle I_s(\vec{\rho},z)\rangle=\langle I_s\rangle$ and hence $\langle I_d(\vec{\rho}_d)\rangle=CA\langle I_s\rangle$. To calculate $\langle I_d(\vec{\rho}_d)^2\rangle$ we assume that the speckle pattern is fully developed.[9] Since the lateral speckle size is diffraction limited and roughly constant throughout the depth of field, the first-order correlation of the speckle intensity can be expressed as[9]

$$\langle I_s(\vec{\rho},z)I_s(\vec{\rho}',z)\rangle=\langle I_s\rangle^2\{1+\mathrm{PSF}_{\mathrm{ill}}(\Delta\rho,0)\}, \quad (2)$$

where $\Delta\rho=|\vec{\rho}-\vec{\rho}'|$.

We introduce the autocorrelation function

$$R_{\mathrm{det}}(\Delta\vec{\rho},z_c)=\int \mathrm{PSF}_{\mathrm{det}}(\vec{\rho}_d-\vec{\rho},-z_c) \times \mathrm{PSF}_{\mathrm{det}}(\vec{\rho}_d-\vec{\rho}+\Delta\vec{\rho},-z_c)\mathrm{d}^2\vec{\rho} \quad (3)$$

[note: $\int R_{\mathrm{det}}(\Delta\vec{\rho},z_c)\mathrm{d}^2\Delta\vec{\rho}=A^2$]. The signal variance is then

$$V(\vec{\rho}_d)=\langle I_s\rangle^2C^2\int R_{\mathrm{det}}(\Delta\vec{\rho},z_c)\mathrm{PSF}_{\mathrm{ill}}(\Delta\rho,0)\mathrm{d}^2\Delta\vec{\rho}. \quad (4)$$

Finally, the rms image is given by $\sqrt{V}$, which depends linearly on fluorescent marker concentration.

To obtain a more quantitative idea of our expected sectioning strength, we use Gaussian–Lorentzian approximations for the illumination and detection PSFs:

$$\mathrm{PSF}(\vec{\rho},z)=\frac{1}{1+\zeta^2}\exp[-2\rho^2/{w_0}^2(1+\zeta^2)], \quad (5)$$

where $\zeta=\lambda z/\pi{w_0}^2$. With this definition, $A=\pi{w_0}^2/2$ and

$$R_{\mathrm{det}}(\Delta\vec{\rho},z_c)=\frac{\pi{w_0}^2}{4(1+{\zeta_c}^2)}\exp[-\Delta\rho^2/{w_0}^2(1+{\zeta_c}^2)]. \quad (6)$$

Finally, the rms at each camera pixel is found to be

$$\mathrm{rms}=\frac{\langle I_s\rangle CA}{\sqrt{3+2{\zeta_c}^2}}. \quad (7)$$

We observe that the rms scales as $1/|z_C|$ for $|z_C|$ larger than the Rayleigh length $\pi{w_0}^2/\lambda$, which indicates that our technique provides depth discrimination. We note that the same sample would give rise to a signal that is constant for a wide-field microscope and scales as $1/(z_C)^2$ for a confocal microscope.[1] Our intermediate technique thus confers quasi-confocal sectioning. (Note that a display of variance instead of rms would lead to confocal sectioning, although at the expense of a nonlinear dependence on marker concentration.)

In practice, the rms image must be derived from a finite sequence of N raw images of intensity I_n, each image corresponding to a different speckle pattern. We use the indicator $[\Sigma(I_{n+1}-I_n)^2/2N]^{1/2}$ to estimate the rms. This indicator is far superior to the more common $[(\Sigma{I_n}^2)/N-(\Sigma I_n)^2/N^2]^{1/2}$ [as prescribed by the definition of $V(\rho_d)$] because it is insensitive to artifactual low-frequency intensity fluctuations caused by the laser or by coarse diffuser inhomogeneities. In particular, our indicator compares each image with only the preceding image, whereas the more common indicator compares each image with the $N-1$ other images.

To confirm our theoretical predictions, we performed DSI imaging of a thin fluorescent plane as a function of axial position z_c. The results (Fig. 2) are found to be in very good agreement with the theory obtained from Eq. (7). The axial resolution can be characterized by the full width at half-maximum (FWHM) of the rms signal, which is roughly $5.4n\lambda/\mathrm{NA}^2$ (n being the index of refraction). This can be compared with the confocal microscope axial resolution FWHM, namely, $1.4n\lambda/\mathrm{NA}^2$. As mentioned above, our technique provides less efficient out-of-focus light rejection than a confocal microscope owing to the slower decrease in signal with z_c.

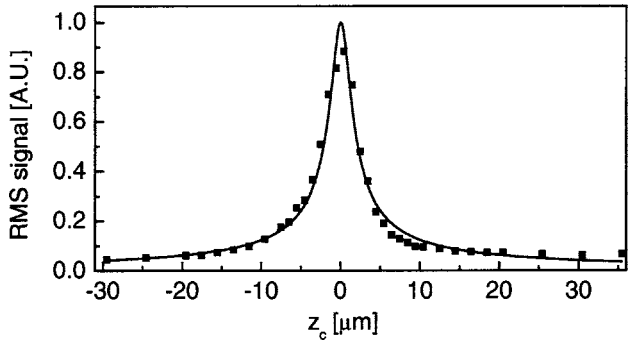

Fig. 2. Theoretical (solid curve) and measured (dots) rms signal from a thin plane of Fluorescein (thickness less than 1.5 μm) as a function of the axial position z_c.

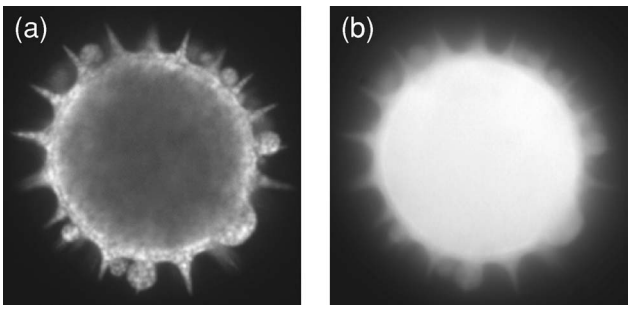

Fig. 3. Simultaneous (a) DSI and (b) conventional wide-field images of a fluorescent pollen grain. The field size is 40 μm $\times$ 40 μm.

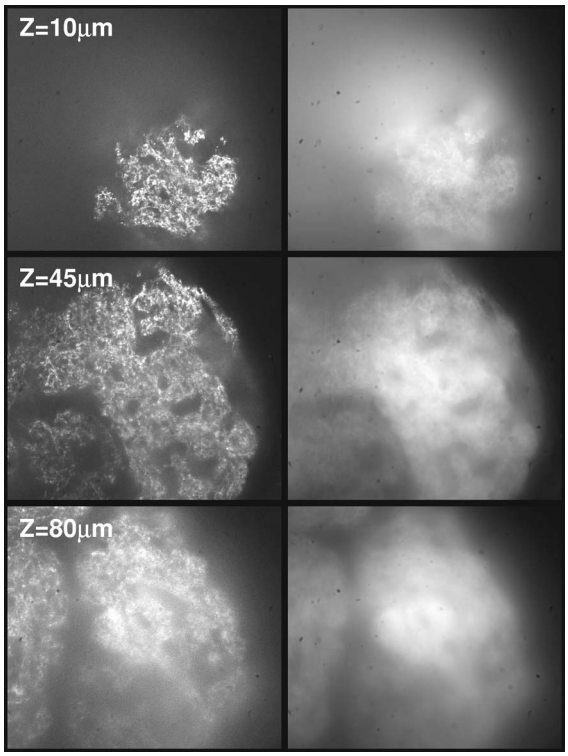

Fig. 4. Simultaneous (left) DSI and (right) conventional wide-field images of GFP targeted to presynaptic terminals of sensory neurons in the glomeruli of an excised (nonfixed) mouse olfactory bulb. The field size is 150 μm $\times$ 150 μm for each image.

We present several images acquired using DSI microscopy. Figure 3(a) shows an image of a pollen grain obtained by computing the rms of 128 raw images (exposure time for each image is 280 ms). We note that the conventional wide-field image can be recovered simply by averaging the raw images. In this way the DSI and conventional images can be displayed simultaneously (Fig. 3). In the rms image, the body of the pollen grain appears darker than the spines, whereas the opposite is observed in the conventional image, demonstrating quasi-sectioning. The rms image can be used to determine the lateral resolution of our DSI microscope: by plotting a profile along a pollen spine, we find a lateral resolution of at least 0.6 μm FWHM.

Finally, we demonstrate that DSI microscopy can be applied to thick tissue imaging. Images of neurons labeled with green fluorescent protein in a mouse brain are shown in Fig. 4. For each image, the rms was calculated from 64 raw images, with an exposure time of 1 s per image (imposed by our low laser power). Comparison with regular wide-field images shows that DSI microscopy rejects most of the out-of-focus blurred light while providing excellent lateral resolution. We found that good image quality was maintained throughout a depth of $\sim$100 μm.

In conclusion, we have demonstrated a new, to our knowledge, technique that provides quasi-confocal fluorescence sectioning. The technique is based on DSI and is very simple to implement with a conventional wide-field microscope. DSI has advantages and disadvantages compared to incoherent structured light illumination. The disadvantages are less-efficient axial sectioning and relatively slow convergence to the correct incoherent image, leading to potential problems with photobleaching (not encountered in our case). In general, residual granularity from the speckle illumination scales as $1/\sqrt{N}$, where N is the number of acquired images, and we found that 50 to 100 images were necessary to obtain a final image of acceptable quality. Nevertheless, the considerable advantage of DSI is that it provides very fine illumination granularity that remains highly contrasted even deep inside scattering media, allowing quasi-sectioned imaging in thick tissue with high spatial resolution. This advantage should prove useful in bioimaging applications.

We thank M. Wachowiak for providing the mouse olfactory bulb sample. This work was funded by the Whitaker Foundation. J. Mertz's e-mail address is jmertz@bu.edu.

References

1. T. Wilson and C. Sheppard, *Theory and Practice of Scanning Optical Microscopy* (Academic, 1984).
2. T. Wilson, R. Juskaitis, M. A. A. Neil, and M. Kozubek, Opt. Lett. **21**, 1879 (1996).
3. M. A. A. Neil and T. Wilson, Opt. Lett. **22**, 1905 (1997).
4. M. A. A. Neil, A. Squire, R. Juskaitis, P. I. H. Bastiaens, and T. Wilson, J. Microsc. **197**, 1 (2000).
5. M. G. Somekh, C. W. See, and J. Goh, Opt. Commun. **174**, 75 (2000).
6. M. C. Pitter, C. W. See, and M. G. Somekh, Opt. Lett. **29**, 1200 (2004).
7. J. Walker, Opt. Commun. **189**, 221 (2001).
8. S. Jiang and J. G. Walker, Opt. Commun. **238**, 1 (2004).
9. J. W. Goodman, *Statistical Optics* (Wiley, 1985).